Instrument Trade Study
Final Report

Advanced Microwave Radiometry and Scatterometry Approaches for Surface Hydrology

Eni G. Njoku[1]
Bill Wilson[1]
Simon Yueh[1]
Yahya Rahmat-Samii[2]

[1]Jet Propulsion Laboratory
California Institute of Technology
Pasadena, CA

[2]Dept. of Electrical Engineering
University of California
Los Angeles, CA

October 21, 1998

Jet Propulsion Laboratory
California Institute of Technology
Pasadena, CA 91109

1. Objectives

Microwave radiometry and scatterometry are preferred techniques for many remote sensing applications, particularly for measurements of soil moisture, snow cover, sea ice extent and motion, sea surface salinity, sea surface temperature, and sea surface wind velocity. Achieving a given spatial resolution for these measurements requires much larger effective apertures at microwave frequencies than at optical and infrared frequencies. It is thus a challenge, for low-frequency microwave systems, to achieve high spatial resolution within necessary limits on payload size and cost.

In this study we have examined techniques and technology options for achieving desired microwave system performance (high spatial resolution and accuracy) using low-mass deployable antennas. We have focused on soil moisture and ocean salinity, as science applications of high priority that drive the requirement for large antennas, and cannot at present be measured adequately from space. System and subsystem performance requirements have been defined, traceable to the science requirements for these parameters, in order to establish detailed technology targets, and to enable planning and prioritization, for a potential space mission.

For soil moisture and salinity sensing, the desired frequencies are in the range 1 to 3 GHz, and our study focuses on this frequency range. However, the concept and technologies evaluated are applicable to all the science parameters listed above, which can be sensed by using additional measurement channels at frequencies up to 14 GHz. The advantage of large aperture systems is that measurements of these parameters can be obtained at much higher resolution than currently feasible.

2. Work Performed

2.1 Science Priorities and Requirements

Soil moisture and ocean salinity are the scientific measurement priorities that drive the requirement for large, spaceborne, remote sensing antennas. Both of these parameters require low-frequency sensing in the 1 to 3 GHz range. This study has focused on a system design and appropriate technologies that meet the science accuracy and resolution requirements for these parameters. The science requirements have been developed from planning documents, science workshops, and discussions with scientific colleagues.

2.2 System Configuration

An optimal system configuration has been developed for a spaceborne mission, based on science requirements for accuracy, stability, spatial resolution, and spatial and temporal coverage. The antenna configuration consists of a low-mass, rotating, offset-fed, parabolic mesh reflector, with multiple multichannel feedhorns. From this configuration, requirements have been derived for subsystems including the reflector, feeds, radiometers, and radar components, in terms of parameters such as receiver sensitivity, calibration accuracy, and antenna pattern gain, cross-polarization, and sidelobes.

2.3 Feed/Reflector Configuration Study

A key aspect of the study has been the design of the combined feed and reflector configuration to provide an optimal trade-off between compactness, antenna beam performance, footprint sampling pattern, and reflector spin rate. Antenna patterns have been computed for the design configuration to verify its performance characteristics.

2.4 Retrieval Simulations

For the optimized configuration, retrieval simulations have been performed for both ocean salinity and soil moisture, to verify that the system design meets the science accuracy requirements, as influenced by anticipated instrument-related error sources and geophysical noise. The simulations have been performed in greater detail for ocean salinity since this parameter places more stringent requirements on the system design. Additional simulations have been performed for alternate designs (fewer channels, cross-track scan) to demonstrate the advantages of the chosen design.

2.5 Aircraft Subsystem Integration and Tests

A dual-polarized microwave L and S-band integrated radar/radiometer aircraft instrument was designed and built during this study using shared funding. Laboratory tests of this instrument have been carried out to verify the anticipated performance of an equivalent spaceborne implementation. Airborne tests of the instrument will be conducted starting in late 1998 or early 1999.

3. Results

3.1 Science Requirements

The summarized science requirements for global soil moisture and salinity sensing are listed in Table 1. The requirements have been derived from recent science working group and agency documents. We emphasize the salinity requirements here since these are the main drivers for the system specifications. The theory and requirements for soil moisture observations are discussed in Georgakakos [1996].

Three broad primary scientific objectives for sea surface salinity (SSS) sensing have been proposed by the Salinity Sea Ice Working Group (SSIWG) [Lagerloef et al., 1998]. These objectives include: (1) Improving seasonal to interannual El Nino Southern Oscillation (ENSO) climate predictions, where assimilating SSS combined with other parameters has been shown to have a positive impact on coupled forecasts; (2) Improving ocean rainfall estimates and global hydrologic budgets, where the oceanic mixed layer freshwater budget is reflected in SSS variability and can be used to balance surface freshwater flux; and (3) Monitoring large scale salinity events, in particular, tracking interannual SSS variability in the Nordic Seas. This variability influences oceanic thermohaline convection and heat transport, and is vital to long term climate prediction and modeling. The specific accuracy requirements for these cases vary with the space and time scales of the phenomena to be resolved. The signal for the ENSO problem is estimated to have length > 100 km, weekly time scales, and a signal strength of 0.05-1 psu. The requirement for the surface water flux problem can be estimated as ~0.05 psu, and 2°x2° monthly resolution in low to mid latitudes. Observing global surface salinity is viewed as a high priority for the National Polar Orbiting Environmental Satellite System (NPOESS) for operational weather forecasting. The NPOESS requirements for global SSS measurements are 0.2-0.3 psu, at better than 100 km resolution, monthly.

The principles as well as technical challenges of satellite SSS remote sensing using low microwave frequencies (1-3 GHz) have been recognized for over two decades [Swift and McIntosh, 1983; Lagerloef et al., 1995]. L-band (1.4 GHz) has been considered to be the best frequency range for ocean salinity measurements, since at this frequency the sea water dielectric constant is quite sensitive to changes in SSS. Changes in dielectric constant influence the sea surface emissivity, which can be sensed by microwave radiometers. Inferring the microwave emissivity from the measured brightness temperature requires a knowledge of the ocean surface temperature. S-band (2.7 GHz) or C-band (6.8 GHz) brightness temperatures can provide the added information on surface temperature necessary for the estimation of SSS. Microwave

brightness temperature measurements performed from the late 1960's through the 1980's have also shown the influence of ocean surface roughness on L- and S-band ocean brightness temperatures. It is highly desirable, therefore, dual-polarized radiometer measurements and/or active radar backscatter measurements be included as part of the remote sensing system, to provide additional data for roughness correction. Two key system design issues are thus: (1) determining via simulations how well SSS can be measured by multichannel satellite microwave systems; and (2) determining the performance specifications required of the microwave sensors for these measurements.

Table 1: Science Requirements

Parameter	Accuracy	Global coverage period	Spatial resolution
Soil moisture	0.04 g cm^{-3} *	3 days	30 km
Ocean Salinity +	0.2-0.3 psu weekly	3 days	100 km

* In the top 2 to 5-cm of soil, where vegetation is less than ~5 kg m^{-2}

+ Benchmark requirement (NPOESS). Requirements of specific applications can be met by space-time averaging (with assumptions on noise correlation).

3.2 System Configuration

The sensor concept studied here has the capability of meeting the science requirements given in Table 1, while also meeting the requirements for a low-cost space mission with a short development cycle. The system characteristics of the concept are given in Table 2.

The radiometers operate at two frequencies (1.41 and 2.69 GHz) and the radar at a single frequency (1.26 GHz). The 1.41 GHz frequency is required to obtain adequate sensitivity to ocean salinity and soil moisture. The 2.69 GHz frequency, and dual polarization, are required to provide corrections for surface roughness and surface temperature over ocean, and vegetation cover over land. The 1.26 GHz radar channels provide corrections with higher sensitivity to ocean roughness and vegetation land cover than can be provided by radiometric channels alone. The exact frequencies and bandwidths chosen are dictated by international frequency-spectrum allocations for passive and active systems.

The antenna concept is a 6-m-diameter rotating, offset-fed, parabolic mesh reflector, with a cluster of three feedhorns. The combined antenna and feed system rotates about the vertical axis with antenna beams offset at a constant angle from nadir, providing a conical scan and wide swath for frequent global sampling. Figure 1 shows the configuration and the conical scan pattern. As the spacecraft moves, the 3-dB antenna footprints provide complete overlap coverage along track and across the swath.

Figure 1 shows the antenna aperture diameter of 6 m. The original baseline for our study was 10 m, and the antenna optimization and pattern computation results (Section 3.3) were performed for the 10-m diameter. However, we subsequently revised the diameter downward to 6-m. (The results of Section 3.3 scale straightforwardly from the 10-m to the 6-m diameter.) The 6-m diameter is a compromise that provides adequate spatial resolution for the science measurements (taking into account the possibility of resolution-enhancement processing for the soil moisture application) while being a feasible first step for a spaceborne demonstration of the low-mass mesh-antenna technology for remote sensing.

Table 2: System Characteristics

Radiometer Frequencies	1.41 GHz	2.69 GHz
Polarization	Vertical and Horizontal	
Antenna Aperture	6 m	
Antenna Beamwidth	2.4°	
Antenna Beam Efficiency	> 90%	
Radar Frequency	1.26 GHz	
Radar Polarization Modes	VV, HH, VH	
Orbit altitude	600 km	
Incidence Angle	40°	
Footprint Size	35 x 45 km	
Swath Width	900 km	
Number of Pixels in Swath	20	
No. Antenna Beams per frequency	3	
Rotation Rate	6.6 rpm	
RMS Noise per pixel (B = 100 MHz)*	0.1 K	
Radiometer Calibration Stability	< 0.2 K	
Radiometer Absolute Calibration Accuracy	1.0 K	
Radar Calibration Stability (1σ)	0.2 dB	
Radar Calibration Accuracy	1 dB	
Radar Transmit Power and Duty Cycle	200 Watts and 10%	
Data Rate	12 Kbits/sec or 120 Mbytes/day	
Power	300 Watts	
Radiometers and Feeds Mass	12 kg	
Antenna Mass	~ 15 kg	

* Over ocean, and averaging forward and rear pixels. Over land, the bandwidths are reduced to 25 MHz and 10 MHz at 1.41 and 2.69 GHz, respectively, to minimize radio-frequency interference.

Each of the three feedhorns is shared between the 1.41 and 2.69 GHz radiometers and the 1.26 GHz radar. The three feedhorns provide three separate beams, allowing the reflector to rotate at the relatively moderate rate of 6.6 rpm. Under-illumination of the main reflector at 2.69 GHz provides roughly equal beamwidths at 1.41 and 2.69 GHz. The rotation rate of 6.6 rpm provides overlap of the footprints on the ground at the 3-dB level (1/2 Nyquist sampling).

There are a number of different structural concepts for mesh deployable antennas. Typically, the mesh is fabricated from 1.2 mil gold-plated molybdenum wire that is knit into a diamond shaped pattern. The required density of the wires is dictated by the RF wavelength. A 10-wire per inch density is commonly used, which provides excellent reflectivity up to X-band and above. The loose nature of the knit allows the individual wires to shift relative to each other when not under tension. This characteristic allows the mesh to be stowed compactly and then stretched to the deployed configuration with minimal short wavelength surface error. The most commonly used "shaping" technique is to use a network of tensioned cables that provide the tie-down structure for

the large number of flexible ties that interface to the mesh reflector. The larger the number of ties, the higher the surface precision. A number of different options can be considered for the rigid outer support structure. These include the "radial rib" and "perimeter truss" concepts. The perimeter truss is a relatively new concept, based on a toroidal-shaped structure that supports the mesh reflector and its surface-shaping network of cables and ties at their outer perimeter. Mesh-deployable antennas in the 12-m-diameter size range, using both radial rib and perimeter truss designs will be launched in 1999 and 2000 for geostationary communication satellite applications [Miller, 1998]. In this study we have not evaluated specific mesh or structural designs.

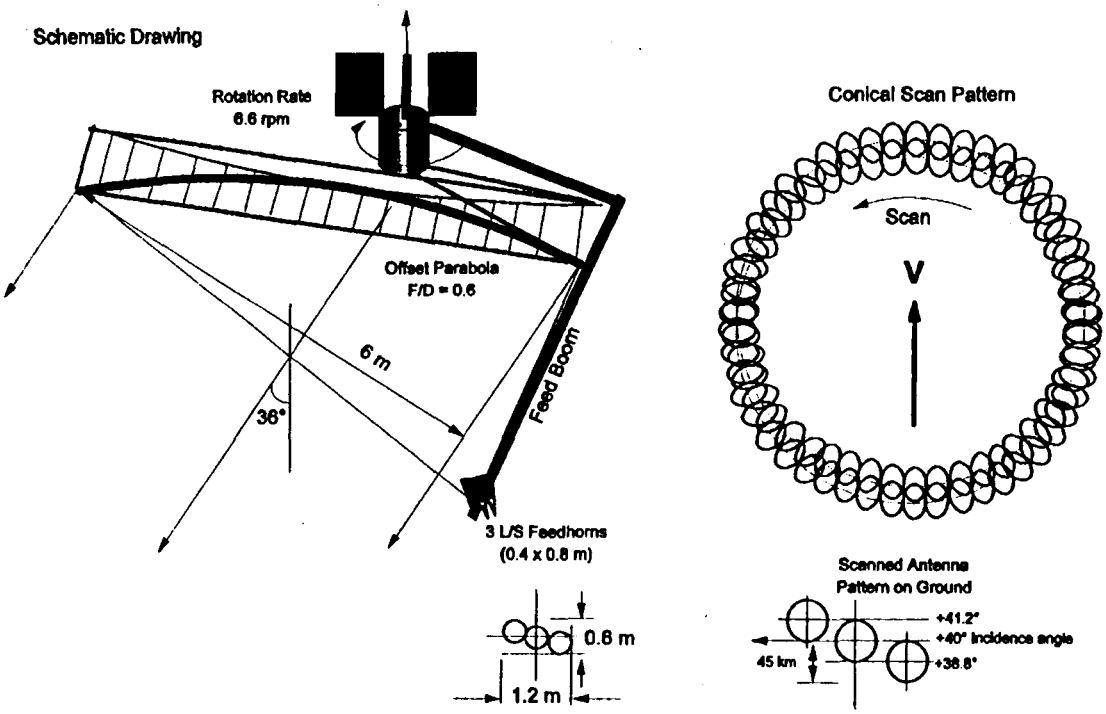

Figure 1: Schematic of the large-aperture, rotating mesh antenna concept.

3.3 Feed/Reflector Configuration Study

Optimum parameters for the feed/reflector configuration have been derived, including focal length, tilt angle, feed dimensions, placements, beamwidths, and cross-polarization levels. Simulated antenna patterns have been generated to illustrate the achievable antenna system characteristics, including beam efficiency, sidelobe and cross-polarization levels, beam shape, and beam width. As mentioned earlier, these computations have been done for an antenna diameter of 10m.

Figures 2 (a) and (b) show the reflector and conical feedhorn geometries and dimensions. The feedhorn is symmetric, and only one half of the section is shown. Figures 3 (a) and 3 (b) show the L and S-band far-field antenna patterns for one of the three beams. The other two beams have similar patterns. Table 3 shows the antenna pattern characteristics, including beam widths and beam efficiencies, for both ideal and conical-horn feeds, and for at-focus and off-focus positions. From these results it is clear that the antenna design can provide more than adequate beam performance.

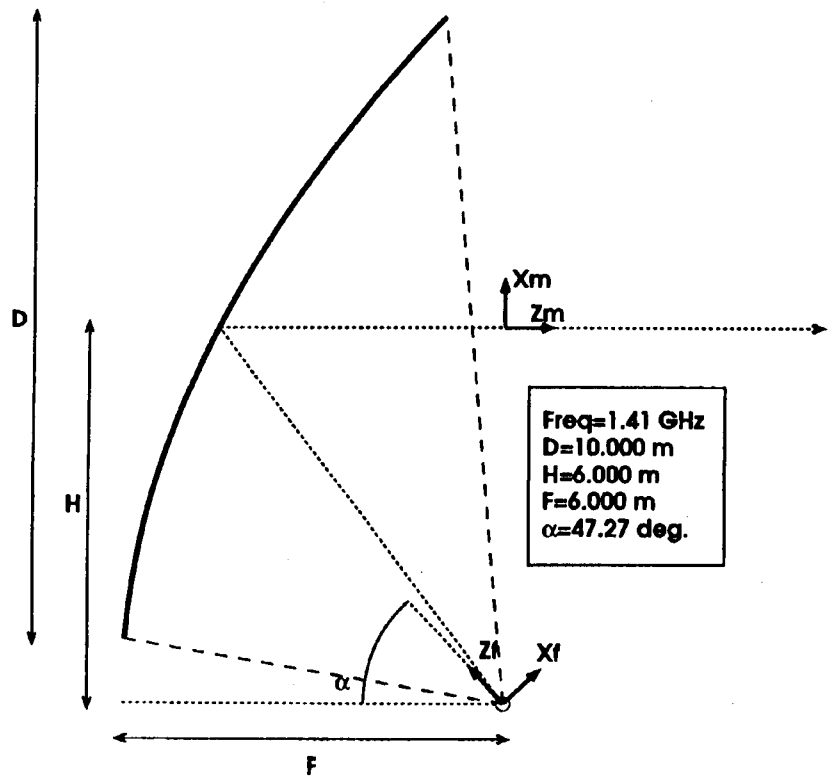

Figure 2 (a): Schematic cross-section of the antenna reflector showing the geometry and optimized dimensions (10-m-diameter antenna shown).

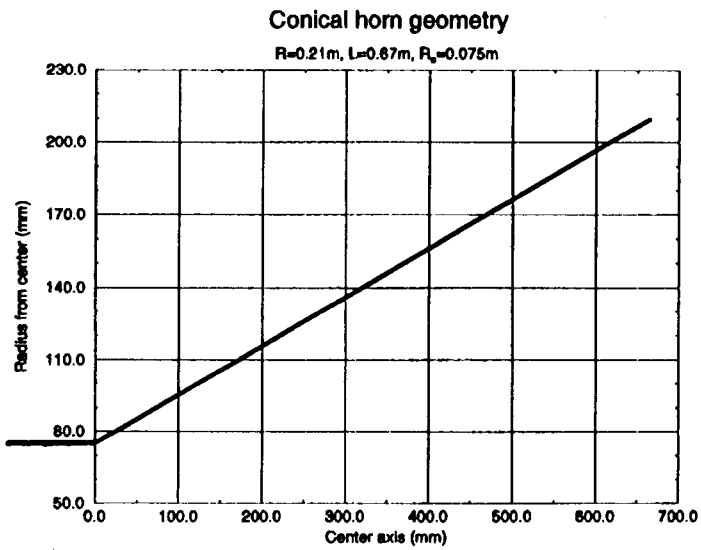

Figure 2 (b): Conical feedhorn geometry and dimensions

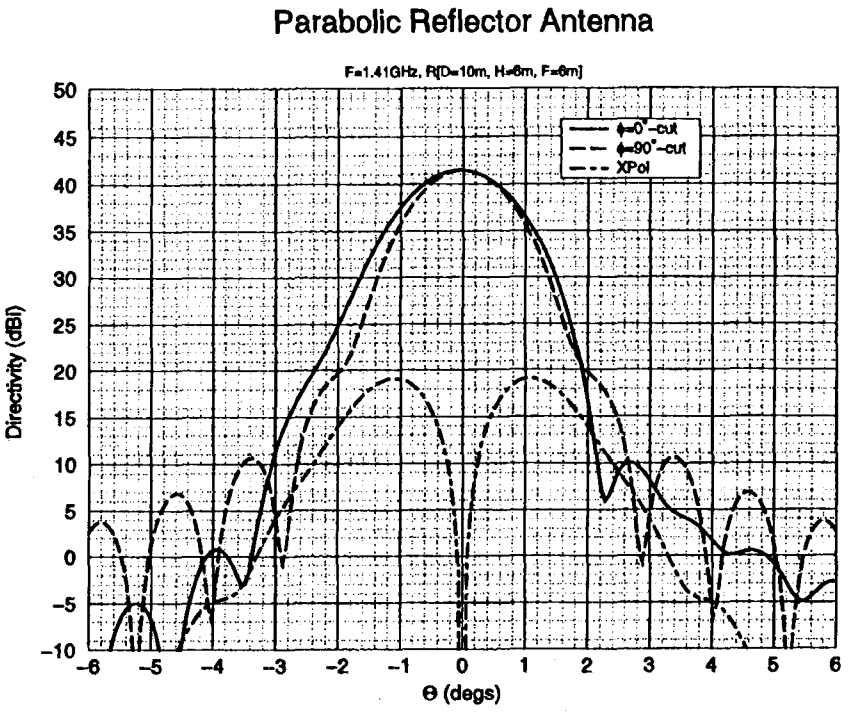

Figure 3 (a): L-band far-field antenna pattern for the 10-m parabolic reflector

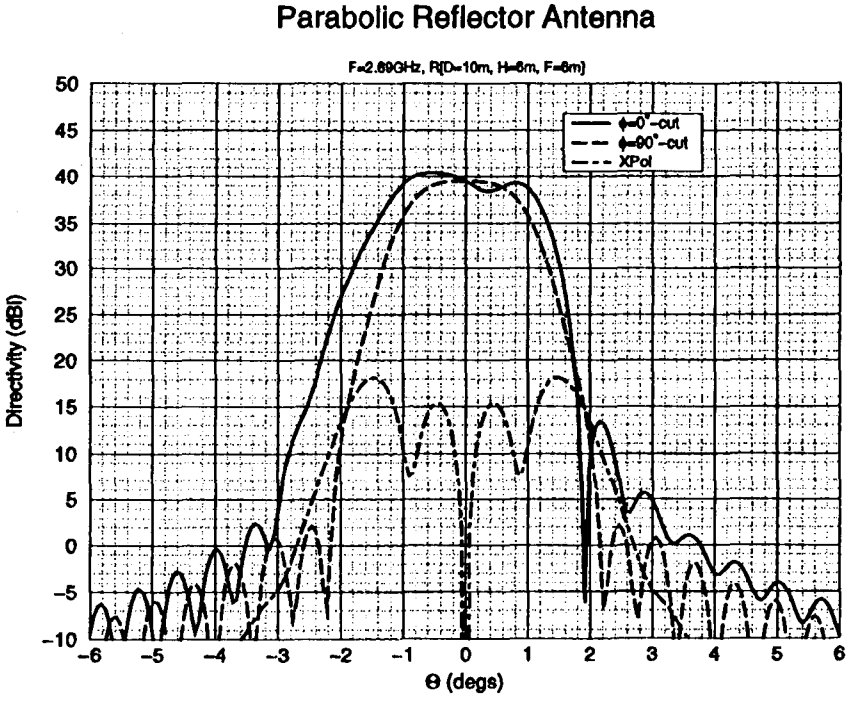

Figure 3 (b): S-band far-field antenna pattern for the 10-m parabolic reflector

Table 3: Antenna pattern performance data (10-m diameter)

SMRM	L-Band				S-Band			
	D [dB]	AE [%]	BW [°]	BE [%]	D [dB]	AE [%]	BW [°]	BE [%]
IH, A-F	42.05	73.59	1.38	95.21	46.16	52.08	1.52	99.85
CH, A-F	41.39	63.20	1.56	90.42	38.62	9.16	1.72	96.40
IH, O-F	41.95	71.88	1.53	95.37	45.76	47.46	1.68	99.87
CH, O-F	41.43	63.79	1.56	89.96	39.47	11.16	1.92	96.51

D = Directivity AE = Antenna Efficiency

BW = BeamWidth BE = Beam Efficiency

IH = Ideal horn feed model CH = Conical Horn Feed

A-F = At Focus O-F = Off Focus ($\Delta x = 0.25$ m, $BT = 1.8°$)

3.4 Retrieval Simulations

An ocean parameter retrieval simulation study has been performed to evaluate the anticipated instrument performance and specifications. This study was based on a performance simulation tool which simulates L and S-band radiometer and radar sensor measurements for given satellite orbit characteristics, instrument design, and calibration performance parameters such as antenna rotation rate, antenna beam pointing accuracy, spacecraft attitude errors, radiometric calibration accuracy, and radiometer bandwidth. Three types of noise were considered, including geophysical modeling noise, sensor calibration errors, and radiometer and radar signal detection sensitivities. Using climatologies of ocean salinity and surface temperature, ECMWF winds, and SSM/I monthly-averaged atmospheric water vapor and cloud liquid water paths as input fields, a set of radiometer and radar simulated measurement data was computed for incidence angles of 40° and 45°. The simulated noisy sensor data were processed using the conjugate-gradient method to retrieve ocean salinity and other geophysical parameters, minimizing a normalized least square measure. The results were averaged over a 7-day period for one set of input fields for the month of May.

The weekly-averaged retrieval results are plotted as a set of color maps which show the global distributions of SSS and SST. Figure 4 shows the input field (ie., the true field), the retrieved field, and the difference between the fields, on separate maps for a 40° incidence angle. Comparing the retrieved fields with the true fields, it is seen that the main features of the SSS and SST fields have been correctly retrieved. The error map exhibits vertical striations which reflect the presence of time-correlated calibration errors in a data set that consists of many relatively narrow swaths.

The SSS retrieval rms errors have also been determined in different latitude bands, at 40° incidence (Figure 5). (The rms errors are similar at 40° and 45° incidence angles.) At higher latitudes, the retrieval error is greater because the ocean temperature is colder. Colder water temperatures exhibit smaller change in L-band brightness temperatures as a function of SSS. Including the L-band radar in the retrieval reduces the rms error by 0.05 to 0.1 psu. The improvement comes from an improved estimate of the surface roughness. The improved accuracy and extra capabilities of the radar must be traded against the increased cost of the system.The results of these simulations show that for 100 km spatial resolutions and 1-week averages, the

Salinity Retrieval Simulation (7 Days of Data)

L-/S-Band Radiometer And L-Band Radar

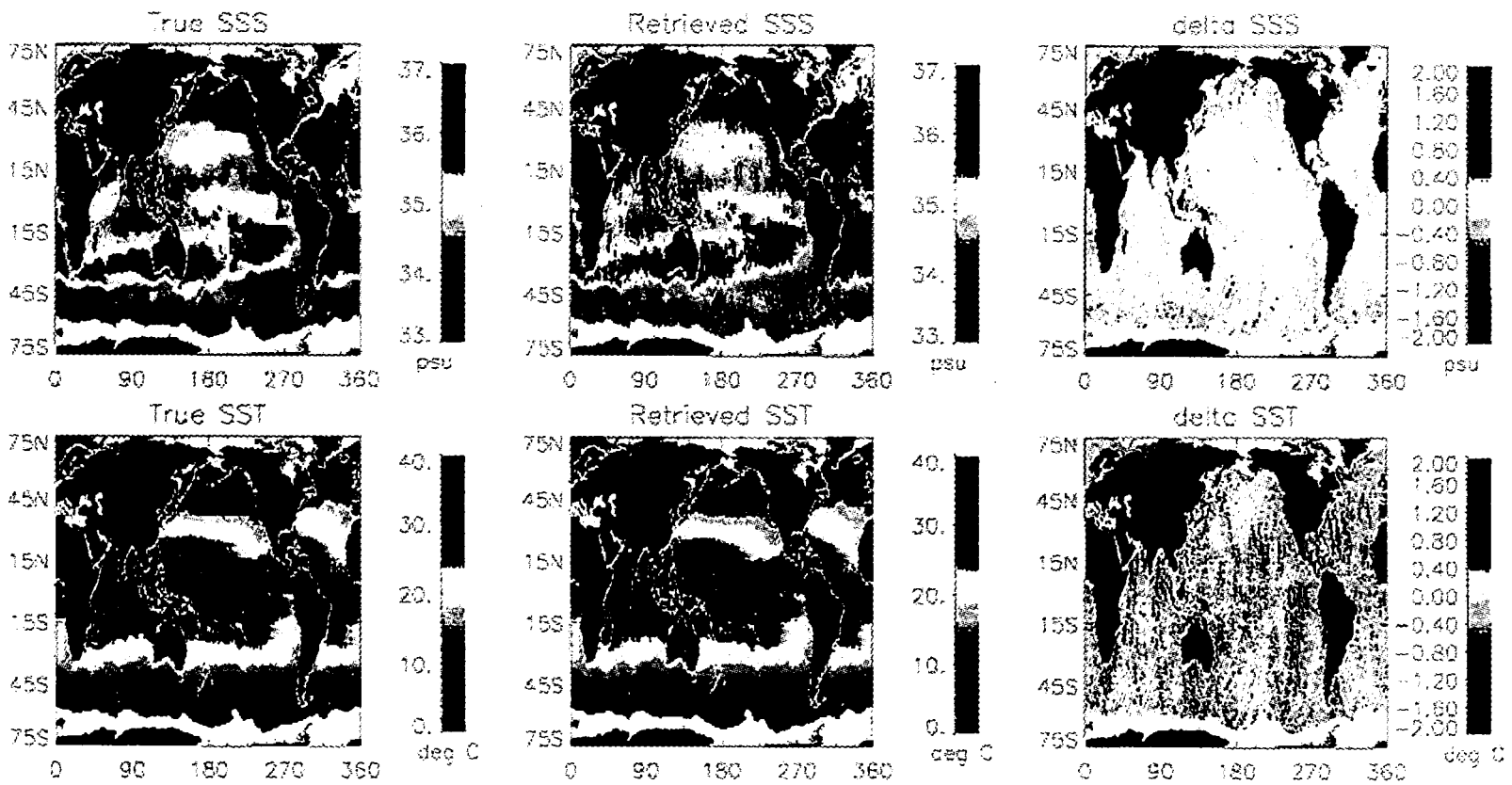

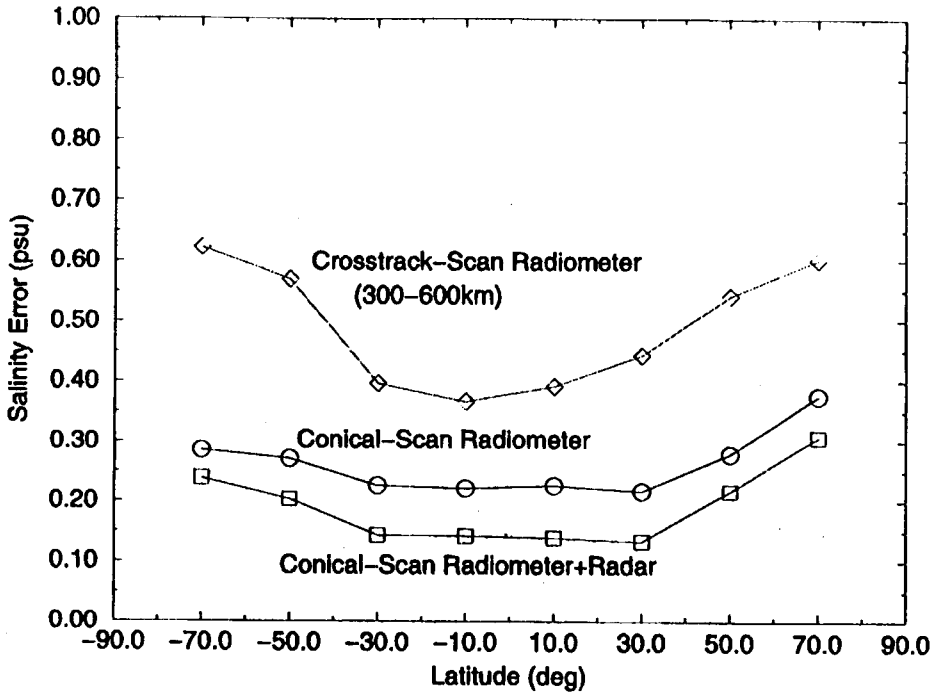

Figure 5: Salinity retrieval simulations (7 days of data), L/S-band radiometer and L-band radar. The salinity retrieval error is shown as a function of latitude for different simulation cases.

salinity measurements are expected to have errors of < 0.15 psu in the tropics and sub-tropics, and ~ 0.3 psu in sub-polar regions. It is expected that additional accuracy can be realized with further space-time filtering and co-analysis with in-situ surface data to resolve weaker signals on longer time scales, such as the Great Salinity Anomaly. This suggests that this instrument concept can meet the stated science requirements assuming reasonable instrument noise and calibration performance. We find that, to achieve the required accuracy for ocean salinity, a radiometer with an RMS noise (ΔT) of 0.1 K per pixel, a calibration stability of 0.2 K and an absolute temperature calibration accuracy of < 1 K is needed. Radar backscatter calibration stability of ~0.2 dB is required. These requirements have been derived for an incidence angle in the range of 40° to 45°.

A further analysis has been performed to estimate how well sea surface salinity (SSS) anomalies of various spatial scales can be measured. The salinity radiometer and radar simulation tool described above was used to analyze an SSS anomaly field generated by the Parallel Ocean Climate Model for the first week of January 1992 [Tokmakian, 1998]. The results suggest that the microwave system under consideration will be able to track many SSS anomalies with magnitudes of a few tenths of psu and spatial scales of a few hundred kilometers in the tropical regions, weekly. The degraded performance for colder waters results in more noisy SSS anomaly retrieval at high latitudes, but a large SSS anomaly (about 1 psu) off Newfoundland is still detectable.

A set of simulations were performed to determine the sensitivity of the retrieval to the characteristics of sensor calibration errors. One simulation assumed a slowly varying calibration error with a correlation time of four minutes and the other assumes a temporal correlation time of eight seconds. A shorter correlation time enables a more significant reduction of the artifacts in the retrieved SSS anomalies in the north and equatorial Pacific. This suggests that a frequent calibration (every few seconds) is desired for a microwave salinity sensor to remove the time varying calibration bias.

Table 4: Calibration Requirements Breakdown

	Stability (1 sigma)			Bias (3 sigma)		
Parameter	Parameter Error	Radiometer (K)	Radar (dB)	Parameter Error	Radiometer (K)	Radar (dB)
Antenna Beam Gain and Pattern		0.1	0.15		2	0.7
Antenna Beam Pointing	0.1°	0.15	0.1	0.3°	0.45	0.3
S/C Attitude	0.01°	0.02	0.01	0.03°	0.05	0.03
Calibration Noise Source	0.1 K	0.1	0	1 K	1	0
Radar Calibration Loop	0.05 dB	0	0.05	1	0	1
Waveguide/ Coax cable loss	0.05 dB	0.05	0.01	0.1 dB	0.1	0.1
RSS		0.2	0.19		2.5	0.9

To assess how well the calibration requirements can be realized, a calibration budget is shown in Table 4. It is assumed that calibration bias can be accounted for by empirical correlation of radiometer and radar observations with in-situ data through adjustment of the geophysical model functions. Thus, the science performance is limited by the stability of the instrument. The antenna beam gain and pattern calibration errors can be limited to less than 0.1 K for a beam efficiency of larger than 90%. The shaping cables and the supporting struts of the mesh reflector are built with composite and temperature insensitive materials and should be thermally stable in orbit. In addition, the position of the struts and the mesh surface can be monitored by optical techniques such as developed for the Shuttle Radar Topography Mission (SRTM). The knowledge accuracy of 0.01° for spacecraft attitude can be achieved by using star trackers. The stability of the noise source for radiometer calibration has been demonstrated for the Jason (TOPEX follow-on) microwave radiometers. The stability of the radar calibration loop has been demonstrated by system and integration testing of the SeaWinds scatterometer (follow-on to NSCAT). The uncertainty of waveguide or coaxial cable loss from the antenna feed horns to the radiometer electronics can be well corrected by careful temperature measurements of the cables. Thus, the microwave system sensitivity and calibration accuracy appears to be adequate for SSS sensing.

The performance of L and S-band radiometry for soil moisture sensing has been evaluated by Njoku et al. [1999]. Using simulated data with modeled noise, soil moisture was retrieved using L and S band frequencies at vertical and horizontal polarizations and at a 40° incidence angle. The results of the simulations showed that, for modeled noise of 0.5 K per pixel, soil moisture accuracies of better than 0.04 g cm^{-3} are achievable for bare and vegetated surfaces (for vegetation up to ~ 5 kg m^{-2}). Since the ocean salinity measurements require that the system have a noise performance of better than 0.2 K per pixel, the system proposed here will easily meet the soil moisture measurement accuracy requirements.

A study was also done of the errors caused by ionospheric Faraday rotation. With corrections using data from the existing network of GPS satellites and ground receivers, brightness

temperature errors can be reduced to less than ~0.2 K (night) and ~1K (day). Polarimetric radiometer channels should be able to reduce the Faraday rotation error to even lower levels.

3.5 Aircraft Subsystem Integration and Tests

Under shared funding, a dual-polarized L and S-band integrated radar/radiometer aircraft instrument has been built at JPL to demonstrate the capability for precision ocean salinity and soil moisture sensing. This is the first instrument to provide simultaneous dual-polarized active and passive measurements at L and S-bands. One of the objectives of this instrument is to provide data to improve existing radiative transfer and backscatter models of ocean and soil surfaces. Another objective is to develop improved algorithms for spaceborne ocean salinity and soil moisture, and for validation of future space instruments.

This aircraft instrument uses two dual-polarized conical horn antennas with high beam efficiencies (~92%) and low sidelobes (< -23 dB). The instrument is designed to be mounted in the NASA Wallops C-130 aircraft, observing out the rear door of the aircraft. The incidence angle is adjustable. At an altitude of 1.8 km, and an incidence angle of 45°, the footprint of the instrument will have a spatial resolution of 1 km. Special care has been taken in the design of the radiometer, to obtain brightness temperatures with an RMS noise of less than 0.1 K and an absolute accuracy of ~0.5 K. The calibration stability is ~ 0.1 K. The dual-polarized L and S-band short pulse radars have a signal-to-noise-ratio (SNR) > 20 dB, with a transmit power of 5 Watts. The characteristics of the instrument are given in Tables 5 and 6, and a block diagram is shown in Figure 6.

Table 5: L and S-Band Aircraft Radiometer Characteristics

Frequencies	1.41 and 2.69 GHz
Antenna Beam Efficiency	~ 92%
Polarization	Horizontal & Vertical
Beam Incidence Angle	30° to 50°
Spatial Resolution (@ 1800 m or 6,000 ft)	1.0 km
RMS Noise per Footprint	0.12 K
Absolute Calibration Accuracy	0.5 K
Calibration Stability	0.1 K

Table 6: L and S-Band Aircraft Radar Characteristics

Frequencies	1.26 and 3.15 GHz
Polarization	HH, VV, VH
Beam Incidence Angle	30° to 50°
Spatial Resolution (@ 1800 m or 6,000 ft)	1.0 km
Transmit Power and Duty cycle	5 Watts and 5%
Signal to Noise Ratio per pixel	> 15 dB
Calibration Accuracy	1 dB

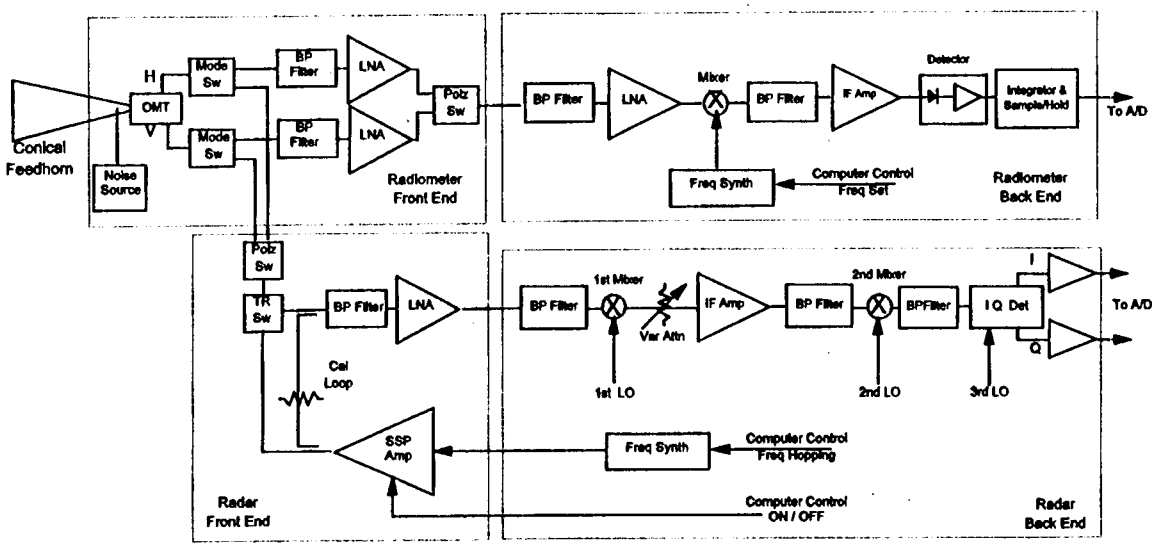

Figure 6: Block Diagram of Dual Radiometer and Radar Instrument

A photograph of the conical horn antennas is shown in Figure 7. The radiometers and radar time-share each antenna and are also switched between polarizations. At the nominal altitude of 1.8 km the radar transmits for 15 micro-seconds then receives for the next 17 micro-seconds. The radar is switched sequentially between the polarizations VV, HH, and VH. The radar pulse repetition frequency (PRF) is 2857 Hz. A solid state amplifier is used for the transmitter, and a calibration loop couples a portion of the transmitted signal (-90 dB) to the radar receiver for calibration. The received radar signal is amplified and down-converted to DC where an I/Q detector is used to measure the in-phase (I) and out of phase components (Q) of the signal. The received power is the squared sum of these signals. All the local oscillators are phase locked to a stable 10 MHz crystal oscillator. The radar signal has a bandwidth of 1 MHz, and both the I and Q signals are sampled at a 2 MHz and converted to a digital signal in the radar computer.

Following the radar receiver range gate, the mode switches to the radiometer for its integration period. The signal is amplified by a low noise amplifier and then down-converted to a 200 MHz IF frequency where it is filtered and detected. This design has the advantage that the radiometer frequency can be tuned manually by the operator to minimize RF interference. The amplified and detected signal is sent to an analog integrator and a sample and hold circuit, and then to the A/D converter in the radiometer computer.

The radiometer integrates ten 300-micro-second periods for each measurement. The radiometer measurement sequence is Antenna V + Noise, Antenna V, Reference load, Antenna H + Noise, Antenna H, Reference load. This triple Dicke switching has the advantage that the radiometer is continuously calibrated every 21 milliseconds. The disadvantage of this switching scheme is that the RMS noise is increased by 20%. However, this is not a problem in an aircraft system with long integration times, and greatly adds to the calibration stability. The noise source is a noise diode with constant current and at constant temperature, that is coupled directly into the feedhorns via a small probe. This provides a very stable calibration signal.

One of the innovations of this system is that all the timing signals are generated by a small timing computer. This computer uses a standard high speed multichannel digital board to generate all the signals for the instrument switches, the data processing circuits and the A/D converters. An advantage of this approach is that it gives flexibility in the design of the switching waveforms, and facilitates modifying the signals if necessary during system testing and checkout.

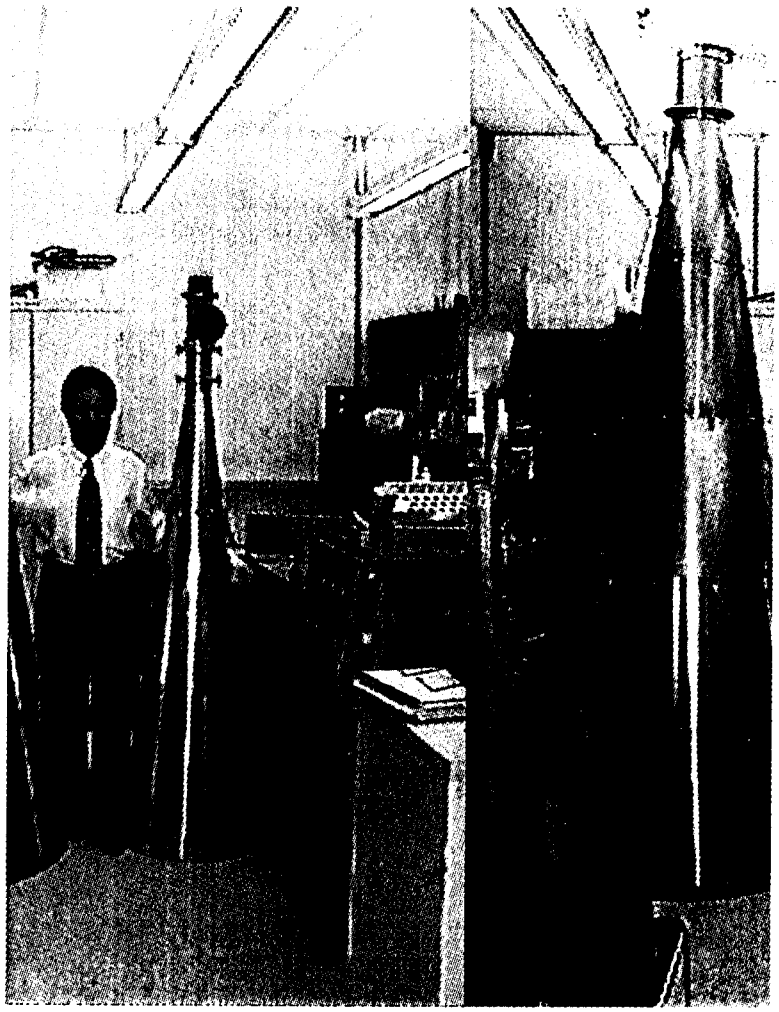

Figure 7: L- and S-band conical horn antennas, with Dr. Rahmat-Samii.

The aircraft instrument has been integrated and is now in the final system testing phase. The first test flights are planned for late 1998 or early 1999.

4. Conclusions and Recommendations

The main conclusions of our study are as follows:

(1) A system configuration has been designed for a multichannel (passive and active) low-frequency microwave spaceborne sensor, operating in the 1 to 3 GHz range, which uses a large-aperture (6-10 m), low-mass, rotating, offset-fed parabolic antenna. The primary science objectives are ocean salinity and soil moisture sensing.

(2) Detailed antenna pattern calculations have been done on the optimized feed/reflector configuration. The results show that the beam performance, in terms of beam efficiency, sidelobes, and cross-polarization, meets the requirements for the ocean salinity and soil moisture sensing applications.

(3) A simulation study has shown that the multichannel, passive and active, constant incidence-angle system is capable of meeting the science spatial resolution and accuracy requirements. Detailed instrument specifications, including requirements on sensitivity, calibration accuracy and stability, and antenna beam performance have been developed, that are necessary to meet the science objectives. These specifications are all within the current state of the art.

(4) A prototype integrated radiometer/radar system has been built and tested in the laboratory. Results show that the instrument subsystems are operating successfully. The instrument is designed for aircraft operation, and will be tested on flights beginning in late 1998 or early 1999. These tests will demonstrate the anticipated performance of a spaceborne radiometer/radar system.

The main recommendations for future work are:

(1) Flight tests of the aircraft system should be continued, over ocean and land targets, to build up a science and engineering database with which to refine and improve the sensor design for a future spaceborne system, and to improve the scientific models on which the retrieval algorithms are based. Funding from Code Y has been obtained, and will continue to be solicited, to support these flights, including ground truth data collection and data analysis.

(2) More detailed studies of the antenna reflector mesh materials, and structural design and dynamics should be conducted, including mesh emissivity, and antenna thermal and mechanical performance under the simulated spaceborne orbital configuration.

(3) A study of the integrated system, including feeds and electronics, boom, antenna reflector, spacecraft, and launch vehicle, should be performed, to provide detailed estimates of feasibility, risk, and cost of a potential spaceborne mission.

** Work on items (2) and (3) will be conducted under the recently-selected Instrument Incubator NRA proposal entitled: "Study of a Spaceborne Microwave Instrument for High Resolution Remote Sensing of the Earth Surface Using a Large-Aperture Mesh Antenna".

5.0 Acknowledgment

This work represents one phase of research carried out by the Jet Propulsion Laboratory, California Institute of Technology, under contract with the National Aeronautics and Space Administration.

6.0 References

Georgakakos, K. P. (1996): Special Issue on Soil Moisture Theories and Observations, *J. Hydrology, 184*, nos. 1 & 2.

Lagerloef, G., Swift, C.T. and Le Vine, D. (1995): Sea Surface Salinity: The next remote sensing challenge, *Oceanography, 8*, No. 2.

Lagerloef, G. (1998): Report of the First Salinity Sea Ice Working Group Workshop, La Jolla, California, 7-8 February.

Miller, B. (1998): Satellites Free the Mobile Phone, *IEEE Spectrum, 35*, no. 3, 26-35.

Njoku, E. G., Y. Rahmat-Samii, J. Sercel, W. Wilson, and M. Moghaddam (1999): Evaluation of an Inflatable Antenna Concept for Microwave Sensing of Soil Moisture and Ocean Salinity, *IEEE Trans. Geosci. Remote Sens.*, (in press: January 1999 issue).

Swift, C. and McIntosh, R. (1983): Consideration for Microwave Remote Sensing of Ocean Surface Salinity, *IEEE Trans. Geosci. Remote Sens., GE-21, No. 4*, 480-491.

Tokmakian, R., A high Resolution Ocean Model with Variable Forcing of Wind, Heat, and Freshwater: Initial Evalution, 1998.